International Journal of Offshore and Polar Engineering (ISSN 1053-5381)

Vol. 30, No. 2, June 2020, pp. 220–227; https://doi.org/10.17736/ijope.2020.jc759

http://www.isope.org/publications

Active Single-Blade Installation Using Tugger Line Tension Control and Optimal Control Allocation

Zhengru Ren and Roger Skjetne
Centre for Research-Based Innovation on Marine Operations (SFI MOVE), Department of Marine Technology
Norwegian University of Science and Technology (NTNU), Trondheim, Norway

Zhiyu Jiang
Department of Engineering Sciences, University of Agder
Grimstad, Norway

Zhen Gao
Centre for Research-Based Innovation on Marine Operations (SFI MOVE), Department of Marine Technology
Norwegian University of Science and Technology (NTNU), Trondheim, Norway

The single-blade installation is a common method for the installation of wind turbine blades. In an offshore installation, a jackup vessel is often involved, and a crane is used to lift, move, and bolt each blade onto the rotor hub at the tower top. To reduce the blade pendular motions, tugger lines are connected to the suspended blade. Active control of the tension force on the tugger lines has been recently investigated to reduce the blade motion. In this situation, a pre-tension is needed during the mating process, as only positive tension can be provided by the tugger lines. To further improve the effectiveness of active force control, we propose an active control strategy with a three-tugger-line configuration in this work. The placement of the third tugger line is examined. The proportional–integral–derivative (PID) control strategy is adopted, and allocation is achieved by convex programming. Aeroelastic simulations are carried out to verify the active control scheme under turbulent wind conditions. The results show that the proposed active control scheme is an effective means of reducing the translational motion of the blade root relative to the hub in the mean wind direction.

INTRODUCTION

Offshore wind turbines (OWTs) have attracted increasing global attention due to their advantages, such as saving land resources and providing superior energy quality. However, during an OWT installation, much time is wasted waiting for the allowable weather window. Hence, OWT assembly and installation are expensive, accounting for 19% of the overall OWT capital expenditures (Moné et al., 2017).

As the blade span exceeds 100 m, the task of lifting an entire rotor assembly offshore may face challenges beyond transportation issues. Single-blade installation, one of many OWT blade installation approaches, involves the lifting of one blade by the main crane and the attaching of the blade to the hub on the top of the turbine tower. The suspended blade and the crane boom are connected by tugger lines, typically without any active control. State-of-the-art single-blade installation is limited to a mean wind speed of 8–12 m/s (Gaunaa et al., 2014). The benefits of the single-blade installation are a wider range of installation vessels, lower crane capacity, and higher deck usage. More efficient lifting and mating operations are required because of the increased number of offshore lifts.

Several publications on various aspects of single-blade installation can be found. The aerodynamic and aeroelastic behaviors of the installation scheme are studied by Gaunaa et al. (2016). The motion characteristics and critical parameters have been investigated (Jiang et al., 2018; Verma et al., 2019a, 2019b). A simulation verification model of single-blade installation for the purpose of control design is proposed in Ren et al. (2018b). To enhance the level of automation and overcome the influence of human operators (Zhen et al., 2019), the control algorithms for optimal lifting operation and stabilizing are proposed and verified with the simulation verification model (Ren et al., 2018a; Ren, Skjetne, and Gao, 2019). Specialized commercial products, such as the LT575 Blade Dragon developed by Liftra and the Boom Lock technology from High Wind have been developed to advance the single-blade installation.

In addition to the blade motion, the motion of the foundation influences the success rate and impact force of the blade's final mating operation (Jiang et al., 2018). In this paper, a monopile foundation is considered the support structure (Jiang et al., 2017). Currently, monopiles are the most cost-effective type of support structure. An offshore structure is exposed to the environmental load effects of current, wind, and waves; hence, the turbine hub motion becomes quite complex (Cheng et al., 2019a, 2019b; Zhou et al., 2019). The dynamics of monopile foundation are presented in Jonkman et al. (2008). High-fidelity hub motion tracking algorithms are presented in Ren, Skjetne, Jiang, et al. (2019). In this paper, a closed-loop feedback control scheme single-blade installation is proposed that uses a proportional–integral–derivative (PID) controller for the tugger line forces.

The paper is structured as follows. The system description and problem formulation are presented in "Problem Formulation," followed by a brief introduction to "System Modeling." The next section discusses the capability of four different configurations of tugger lines. Additionally, a PID controller and an online control allocation based on convex programming are proposed. In "Simulations," simulations are conducted using HAWC2 coupled to a

Received November 2, 2018; updated and further revised manuscript received by the editors August 3, 2019. The original version (prior to the final updated and revised manuscript) was presented at the Twenty-eighth International Ocean and Polar Engineering Conference (ISOPE-2018), Sapporo, Japan, June 10–15, 2018.

KEY WORDS: Single-blade installation, PID controller, wind turbine installation, control allocation, offshore wind turbine, marine operation, crane, coupled simulation.

MATLAB/Simulink interface for the developed controller. Verification of the control scheme using both the simplified model and the high-fidelity model is performed. A set of comparative studies is conducted to demonstrate the active controller performance. The final section presents conclusions and recommendations for future studies.

Notation

$|x|$ and $\|x\|_A$ stand for the Euclidean norm and the weighted Euclidean norm, respectively; i.e., $|x|^2 = x^\top x$ and $\|x\|_A = x^\top Ax$. The bar operator, $\bar{\cdot}$, stands for the mean value over a period.

PROBLEM FORMULATION

Description of Single-Blade Installation

The monopile, transition piece, tower, nacelle, and blades have been assembled before the installation procedure. Before the blade installation begins, the hub is rotated to a horizontal position. Next, the blade is equipped with a yoke at its center of mass and lifted by the crane from the deck to the hub height. The blade root motions are monitored. If the relative displacement and velocity between the blade root and hub are within the allowable limits, then the mating process follows. Figure 1 illustrates a typical mating phase between the blade and the hub. Wind-induced blade motions are controlled by the tugger lines. The mating process is finished when the guiding pins on the blade root have entered the flange holes on the hub. The blade is then bolted onto the hub, and the lifting gear is retracted. A detailed description of the procedure can be found in Jiang et al. (2018).

Problem Statement

In practice, the blade's final installation stage may not be as smooth as described above, especially under high wind speeds. A typical single-blade installation scenario is illustrated in Fig. 2. The leading edge of the blade faces downward with a $-90°$ pitch angle. This blade orientation does not have minimal loading, but it is often adopted in practice because of concerns about transportation and loading predictability when the wind direction changes (Kuijken, 2015). One lift wire is used to rigidly connect the hook and crane tip, and two slings are used to connect the hook and yoke. For the sake of simplicity, only horizontal restoring-force

Fig. 1 Illustration of the mating phase during a single-blade installation [courtesy of RWE AG (2014)]

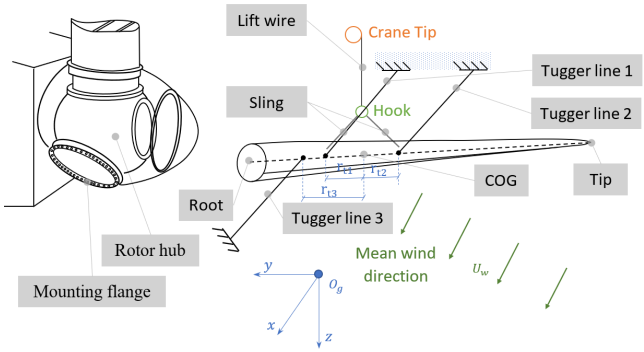

Fig. 2 Single-blade installation configuration in this paper

components from the tugger lines are considered. A three-tugger-line configuration is proposed; i.e., three horizontal tugger lines are connected to the yoke–blade system with arm lengths of r_{t1}, r_{t2}, and r_{t3} relative to the blade center of gravity (COG). These lines help to limit the blade pendulum motions in the horizontal plane. Typical two-tugger-line installation configurations have been considered in Kuijken (2015), Jiang et al. (2018), and Ren et al. (2018a). The tension on the tugger lines can be measured by tension cells and controlled by the winch servo motors. Pretension can be exerted by shortening the tugger lines, resulting in a deviation of the blade COG position from the static position in the air. The configuration of three tugger lines can be realized using off-the-shelf industrial devices. The third line can be connected to the corresponding winch servo motor through pulleys. The motor can be placed on the crane together with the motors for the other two lines.

The global reference frame $\{G\}$ is utilized. The origin O_g is placed at the mean water level with the x-axis pointing in the mean wind direction, the z-axis pointing downward, and the y-axis following the right-hand rule. The rotations about the x-, y-, and z-axes are named roll (ϕ), pitch (θ), and yaw (ψ), respectively.

Gravity is balanced by the lift wire since the blade is seized at its COG. The impact of the wind-induced lift force on the blade vertical motion is very limited. The aeroelastic simulation results in Jiang et al. (2018) illustrate that the three planar motions are critical for a single-blade installation operation in a turbulent wind field, i.e., surge (x), sway (y), and yaw (ψ). The motion on the x-axis is critical because a large wind-induced force is exerted on the yoke–blade system. The wind-induced forces acting on the blade are uneven, and the blade experiences a yaw angle of ψ, as shown in Fig. 2. Additionally, the wind-induced force in the longitudinal direction is quite small compared to the drag force in the mean wind direction; refer to Ren et al. (2018b) for details. Suppose that the tugger lines are horizontally arranged with no vertical force components; then, the horizontal tension in each line can then be denoted by f_1, f_2, and f_3. It is assumed that f_1, f_2, and f_3 are constant on the x-axis. The turbulent wind continuously affects the loading situation of the blade. Therefore, a 6 degrees-of-freedom (6DOF) problem is transferred into a 2DOF problem for a single-blade installation operation. The control objective is to control the blade COG to track the desired setpoint $r_d = [x_d, \psi_d]^\top$ by controlling the force inputs, f_1, f_2, and f_3. The goal is to reduce the motion of the root center in order to ensure the mating operation.

SYSTEM MODELING

It is assumed that a jackup vessel with cranes will perform the blade installation task. The jackup vessel and the crane are

assumed to be rigid; therefore, no external loads on them are modeled. However, the aerodynamic loads on the lifted blade and the induced blade motions are considered. Moreover, the displacements of the nacelle due to the hydrodynamic loads on the monopile are modeled.

Environment

Irregular waves were generated using the JONSWAP spectrum (DNV, 2000). The hydrodynamic loads on the monopile are calculated using Morison's equation. The current velocity is assumed to be constant during the period of operation.

Mann's turbulence model is adopted to simulate the turbulent wind field (Mann, 1998). The wind speed vector at a point in space is a sum of the mean wind velocity and a turbulence. The aerodynamic load on the blade is calculated based on the cross-flow principle, i.e., an integration of the lift and drag forces along the spanwise direction. The wind load in the spanwise direction is negligible. The aerodynamic effect of dynamic stall is not considered, but static stall is inherently accounted for by using the lift and drag curves of the airfoil.

Blade Model

The NREL 5MW wind turbine is selected as the objective of installation.

Tugger Lines

Tugger lines are modeled as springs, which only provide tension forces in the axial direction of the wire.

Monopile Foundation and Support Structures

Various simplified models and high-fidelity simulation models for dynamic load and response analysis of monopile foundations have been investigated in earlier studies, e.g., Jonkman et al. (2008). Here, a distributed model, the Winkler approach, is adopted for monopile–soil interaction. The soil, modeled as plastic material, is layered with different properties, i.e., the effective weight and angle of internal friction. According to the *p-y* model, the soil resistance p is a function of the pile displacement y at a given depth along the pile. Each layer is modeled as an uncoupled nonlinear spring with corresponding stiffness; see Fig. 3. Timoshenko beams are used to model the pile, the transaction piece, and the tower (Bhattacharya and Adhikari, 2011). The waves enter from 30° north of east.

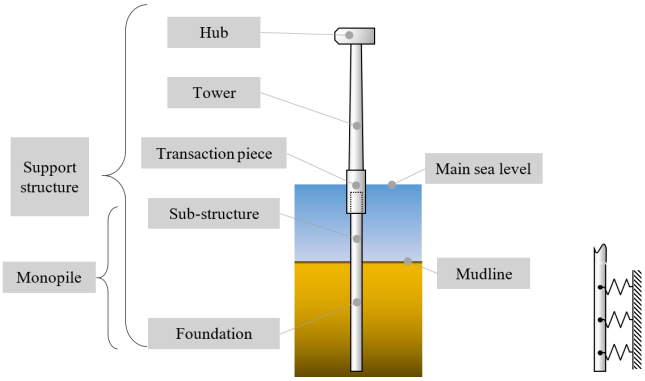

Fig. 3 OWT with monopile foundation (left) and distributed spring model (right)

CONFIGURATION OF TUGGER LINES AND CONTROL ALLOCATION

PID Controller

A PID control algorithm for tugger line tension is used to stabilize the blade's motion (Åström and Hägglund, 1995). The control law is given by

$$\tau_c = \begin{bmatrix} F_{tx} \\ M_{tz} \end{bmatrix} = -K_p \begin{bmatrix} x - x_d \\ \psi - \psi_d \end{bmatrix} - K_d \begin{bmatrix} u \\ r \end{bmatrix} - K_i \int \begin{bmatrix} x - x_d \\ \psi - \psi_d \end{bmatrix} dt \quad (1)$$

where F_{tx} and M_{tz} are the commanded force and torque acting on the suspended blade on the x-axis and the z-axis, and $K_p, K_d, K_i \in \mathbb{R}^{2\times 2}$ are the proportional, derivative, and integral diagonal gain matrices, respectively.

Tugger Lines Configuration

As the tugger lines can only provide non-negative force inputs to the suspended blade, the control input vector $[F_{tx}, M_{tz}]^\top$ is limited by the capability of the crane and winches. In this paper, it is assumed that the placement of the first and second tugger lines follows the typical configuration with $r_{t1} = -r_{t2}$; i.e., they are assembled symmetrically on each side of the blade COG, and they both provide tension forces in the direction opposite to the mean wind direction. The third tugger line is free to be placed in a range (e.g., $-10 \le r_{t3} \le 10$), and it should provide tension force in the mean wind direction.

Suppose that the force input limits are the same for all the tugger lines. Hence, the allowable tugger line control set is

$$\mathbb{D}_f = \{f \mid 0 \le f \le f_{\max}\}, \quad f_i \in \mathbb{D}_f, \quad i \in \{1, 2, 3\} \quad (2)$$

where $f_{\max}$ is the upper limit of f.

A comprehensive analysis is conducted to determine the configuration of the third tugger line. The free-body diagram of a three-tugger-line configuration is shown in Fig 4. The wind-induced load acting in the longitudinal direction is negligible. Hence, only the wind speed component perpendicular to the blade's longitudinal axis is of importance. The wind direction remains close to the mean direction in a short time interval, e.g., 10 minutes. The installation vessel should adjust its heading and position according to the weather forecast and historical data. The overall control configuration is then given by

$$\begin{bmatrix} F_{tx} \\ M_{tz} \end{bmatrix} = \begin{bmatrix} 1 & 1 & -1 \\ r_{t1}\cos\psi & r_{t2}\cos\psi & r_{t3}\cos\psi \end{bmatrix} \begin{bmatrix} f_1 \\ f_2 \\ f_3 \end{bmatrix} \quad (3)$$

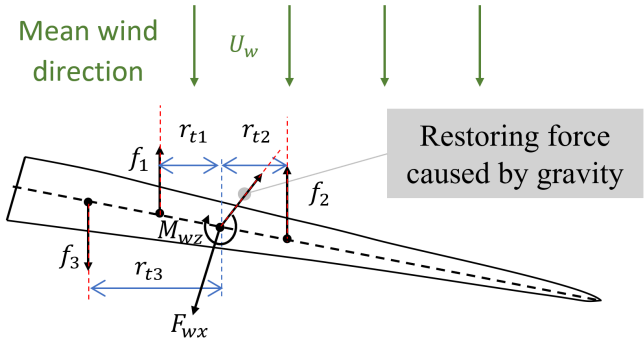

Fig. 4 Free-body diagram in the horizontal plane

In vector form, this is written

$$\tau = Bf \tag{4}$$

where $\tau = [F_{tx}, M_{tz}]^\top \in \mathbb{R}^2$ is the commanded load vector on the blade resulting from the tugger line force vector $f = [f_1, f_2, f_3]^\top \in \mathbb{D}_f^3$, and B is the tugger line configuration matrix. Control allocation is now the inverse problem of Eq. 5; that is, allocating commanded force vector $f_c \in \mathbb{R}^3$ for the tugger lines gives a commanded load vector $\tau_c \in \mathbb{R}^2$, according to

$$\tau_c = Bf_c \tag{5}$$

where $f_c = [f_{c,1}, f_{c,2}, f_{c,3}]^\top$ is the control command vector.

Based on the quasi-static results of the wind-induced force in the mean wind direction and moment about the z-axis for a vertically arranged blade, F_{wx} and M_{wz}, follow quadratic relations, i.e.,

$$\begin{bmatrix} F_{wx} \\ M_{wz} \end{bmatrix} = \begin{bmatrix} k_{F_x} \\ k_{M_z} \end{bmatrix} U_w^2 \tag{6}$$

where $k_{F_x} = -0.174\ \text{kN}\cdot\text{s}^2/\text{m}^2$ and $k_{M_z} = -1.474\ \text{kN}\cdot\text{s}^2/\text{m}^2$ for an NREL 5 MW reference turbine blade. They are calculated by curve fitting based on the results in Ren et al. (2018b).

Here, two domains are defined. The first domain, the control input domain, is the feasible region of the control inputs caused by the tension on the tugger lines, i.e.,

$$\mathbb{D}_c = \left\{\tau \in \mathbb{R}^2 \mid \tau = Bf, f \in \mathbb{D}_f^3\right\} \tag{7}$$

The second domain, the required input domain, contains the control input required to compensate the wind-induced load acting on the blade and is defined by

$$\mathbb{D}_r = \{[F_{wx}(U_w), M_{wz}(U_w)]^\top | U_w \in \mathbb{D}_w = [U_{w,\min}, U_{w,\max}]\} \tag{8}$$

where $U_{w,\min}$ and $U_{w,\max}$ are the minimum and maximum inflow speeds. For a given mean wind speed and turbine class, the wind-induced loads can realistically be compensated by the control inputs from the tugger lines if $\mathbb{D}_r \subseteq \mathbb{D}_c$. In the following, the placement of the connecting points of the tugger line on the yoke is discussed.

The Control Input Domain $\mathbb{D}_c$ with Respect to the Placement of the Third Tugger Line. The tugger line configuration is illustrated in Fig. 4, which shows the force vectors and positions of tugger lines 1, 2, and 3. The third tugger line is placed in the direction opposite that of the other two tugger lines. The distance between its connecting point to the COG on the blade longitudinal axis is r_{t3}; e.g., $-10 \le r_{t3} \le 10$. A series of control input domain tests are conducted with parameter sweeps. The simulation results are presented in Figs. 5–8.

Below are some summaries of $\mathbb{D}_c$:

- It is obvious that $\mathbb{D}_c$ for the three-tugger-line configuration (Fig. 8) is much broader than that for a two-tugger-line arrangement (Figs. 5–7).
- The shapes of $\mathbb{D}_c$ for the configuration with the two-tugger-line configuration are rhombuses, while the shapes of $\mathbb{D}_c$ for the three-tugger-line configurations are hexagons.
- Typically, the choice of the two tugger lines is lines 1 and 2, as seen in Fig. 4. From the proposed results, $\mathbb{D}_c$ is then small. The $\mathbb{D}_c$ for tugger lines 1 and 3 (Fig. 6) and 2 and 3 (Fig. 7) are symmetric about the F_{tx}-axis. The farther the third tugger line is placed from lines 1 or 2, the broader a $\mathbb{D}_c$ can be achieved.
- $\mathbb{D}_c$ can be modified with the tugger line force input upper limitation $f_{\max}$.

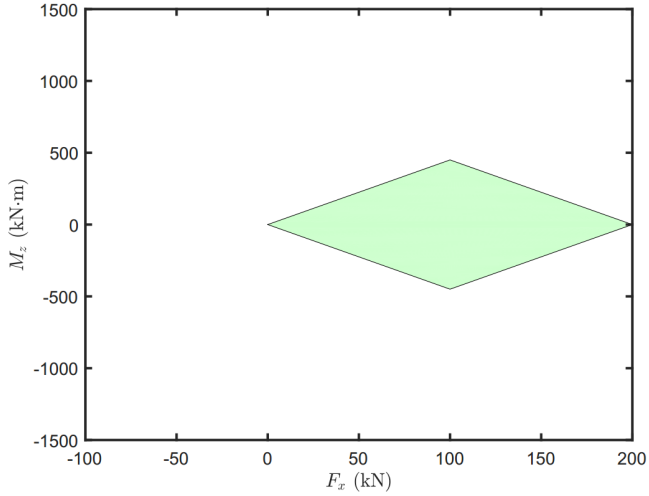

Fig. 5 Control domain with tugger lines 1 and 2 ($f_1, f_2 \in [0, 100]$ kN and $f_3 = 0$)

The Required Input Domain $\mathbb{D}_r$ with Respect to Mean Wind Speeds and Turbine Classes. According to IEC (2005), the normal turbulence model (NTM) is given by

$$\sigma_1 = I_{\text{ref}}(0.75U_w + b), \quad b = 5.6 \tag{9}$$

where $I_{\text{ref}} = 0.16$ for wind turbine class A, $I_{\text{ref}} = 0.14$ for wind turbine class B, and $I_{\text{ref}} = 0.12$ for wind turbine class C. For a normal distribution, the possibility within the wind speed set $\mathbb{D}_w = \{U_w | \bar{U}_w - 3\sigma_1 \le U_w \le \bar{U}_w + 3\sigma_1\}$ is 99.8%. Therefore, the required control input can be calculated based on Eq. 6, assuming that $\bar{U}_w - 3\sigma_1$ and $\bar{U}_w + 3\sigma_1$ are the lower and upper limits for the wind speed. The results are presented in Fig. 9.

Some results are summarized as follows:

- For the Class A wind turbine, $\mathbb{D}_r$ is broader than that for Class B, and they are both broader than that for Class C.
- It is impossible to compensate for the wind-induced loads without pre-tension in the two-tugger-line scheme with tugger lines 1 and 2.

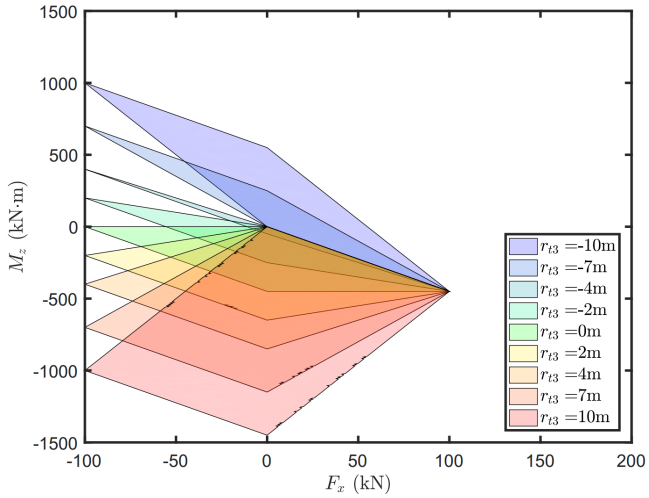

Fig. 6 Control domain with tugger lines 1 and 3 ($f_1, f_3 \in [0, 100]$ kN and $f_2 = 0$)

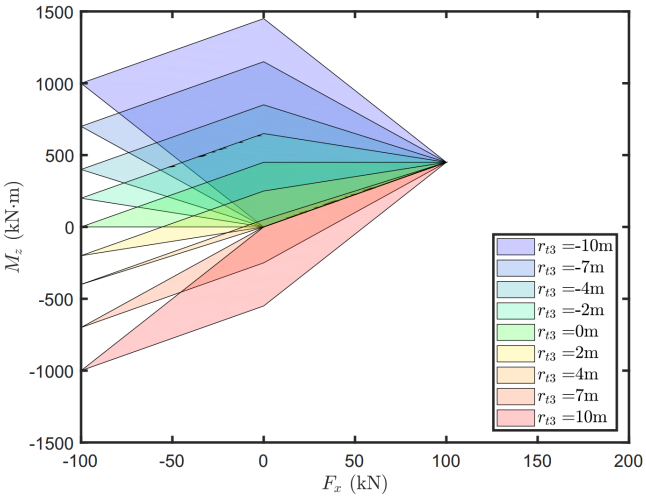

Fig. 7 Control domain with tugger lines 2 and 3 ($f_2, f_3 \in [0, 100]$ kN and $f_1 = 0$)

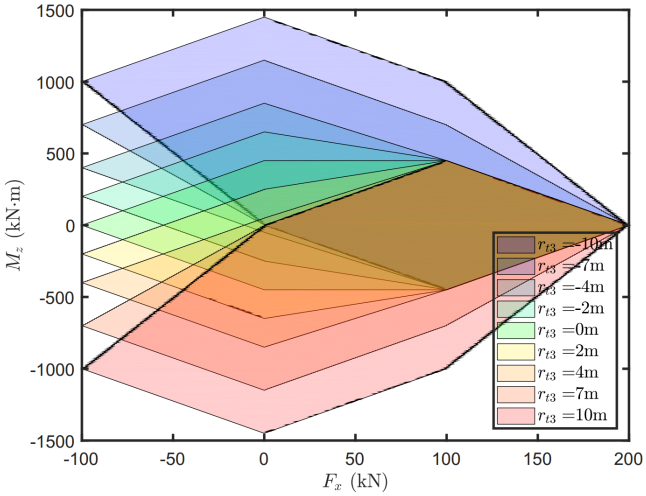

Fig. 8 Control domain with all three tugger lines ($f_1, f_2, f_3 \in [0, 100]$ kN)

• The two-tugger-line scheme with tugger lines 1 and 2 or 2 and 3 can compensate for the wind-induced loads when the mean wind speed and turbulence intensity are limited in range.

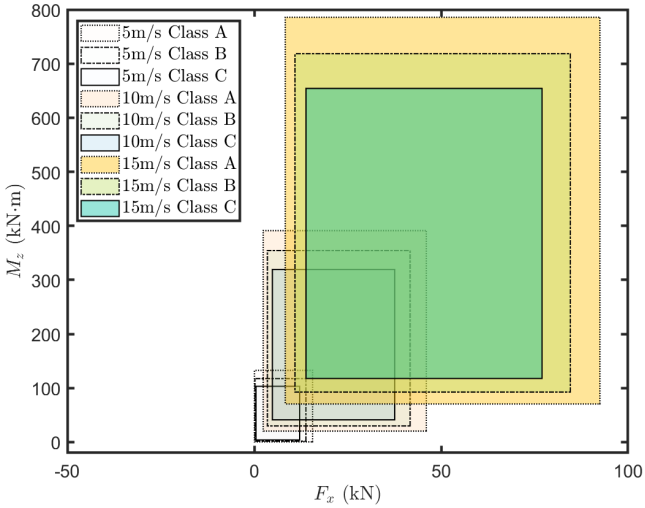

Fig. 9 Required input domain for different wind turbine classes (Class A, B, and C) and mean wind speeds ($\bar{U}_w = 5, 10, 15$ m/s)

• The three-tugger-line configuration with the third tugger line connected to the yoke near the root is the best option for the proposed installation scenario.

In Ren et al. (2018a), tugger lines 1 and 2 are used. The pre-tension, which is needed to achieve negative control input, moves the control scope in the negative F_y direction. Therefore, the control performance is limited by the pre-tension. When the pre-tension is insufficient and the wind-induced loads are so high that the force on the tugger line 1 becomes 0, the system becomes unstable. To stabilize the blade without pre-tension, a three-tugger-line scheme is adopted in this paper.

Control Allocation

Because there are three force inputs (f_1, f_2, and f_3) and only two control inputs (F_{tx} and M_{tz}), the control allocation is an overdetermined problem. The problem is to find f_c from the desired τ_c, according to Eq. 5. However, the typical pseudo-inverse, $f_c = B^{\dagger}\tau_c$ with $B^{\dagger} = (B^{\top}B)^{-1}B^{\top}$, is not applicable since there exists a constraint for each force input, $f_i \in \mathbb{D}_f$, $\forall i \in \{1, 2, 3\}$. In this paper, an online optimization solver is used to handle this constrained overdetermined control allocation problem (Deng et al., 2019, 2020; Johansen and Fossen, 2013). Because the computational demands here are not high, a solver written in the C language is fast enough to realize the online application. There are various programming solvers to handle such programming problems. CVXGEN, an online quadratic program optimization code generator, is applied in this paper (Mattingley, 2011). The programming question is

$$\min_{f_c}\left(\|Bf_c - \tau_c\|_{Q_1} + \sum_{i}^{n_b}\|f_c - F_i\|_{Q_2}\right) \tag{10}$$

subject to $0 \le f_{c,i} \le f_{\max,i}$, $i = 1, 2, 3$, where $Q_1 \in \mathbb{R}^{2\times2}$ and $Q_2 \in \mathbb{R}^{3\times3}$ are the weighting matrices in the objective function. $\mathcal{F} \in \mathbb{R}^{3\times n_b}$ is a buffer matrix to store the previous data that F updates for each time instant after finding the optimal solution f_c^* of Eq. 10; F_i is the ith column of $\mathcal{F}$; and n_b is the number of buffer-stored time instants.

The updated law is given by

$$\mathcal{F} = [\mathcal{F}_{2:n_b} f_c^*] \tag{11}$$

where $\mathcal{F}_{2:n_b}$ contains the $n_b - 1$ newest columns of matrix F. The aim of introducing matrix F is to avoid sudden changes and ensure smooth trajectories of the commanded tension force $f_{c,i}$. The values of the diagonal elements in Q_2 should be much smaller than those in Q_1 for the case in which the tension updating slows.

Actuator Dynamics

Whether the desired tugger line forces can be supplied in time depends on the actuator characteristics. Due to the physical limitations of the actuators, the control signals cannot reach every desired value or rate (Egeland and Gravdahl, 2002). In this study, the actuator dynamics are simplified as stable first-order dynamics, which can be expressed in the frequency domain by the transfer function

$$\frac{f_{i(s)}}{f_{\{c,i\}(s)}} = \frac{1}{T_{fi}s + 1}, \quad i \in \{1, 2, 3\} \tag{12}$$

where T_{fi} is the time constant of the lowpass filter, $f_{c,i}$ denotes the control input command signal from the proposed controller and allocation algorithm f_c, and f_i is the actual physical tugger line force applied to the system at a specific time.

A discrete form of this lowpass filter in the time domain is

$$f_i(t_k) = (1 - a_i) f_i(t_{k-1}) + a_i f_{c,i}(t_k), i \in \{1, 2, 3\} \quad (13)$$

where t_k is the time at the kth sample instant with a fixed sampling interval h and $a_i = h/(T_{fi} + h)$.

SIMULATIONS

Overview

Numerical simulations are conducted in HAWC2 using MATLAB Simulink to control the external force inputs. Selected properties of the blade installation model and the controller parameters are summarized in Table 1. The blade of the NREL 5MW reference wind turbine is used (Jonkman et al., 2009).

A turbulent wind field with a turbulence Class C and a mean wind speed of $U_w = 12$ m/s is adopted in the simulations. The turbulence intensity (TI) is calculated according to the IEC (2005). The turbulence is simulated with Mann's turbulence model. Each simulation lasts 1,000 s. In the response statistics, the first 400 s are removed during post-processing to avoid the start-up transient effect. We select the mean wave direction to be the same as the mean wind direction, with the significant wave height 2 m and wave period $T_p = 6$ s. For a given pair of H_s and T_p, the wave angle of attack is selected as the most critical angle, where the hub motion in the wind inflow direction is the largest.

The criteria are the absolute/relative blade root center's motion radius (Jiang et al., 2018), which is defined by the square root of the sum of motion in the vertical and flow-wise directions. The absolute blade root center's motion radius η_{r0} and the relative blade root center's motion radius η_{rh} are defined by

$$\eta_{r0}(t) = \sqrt{(x_r - \bar{x}_r)^2 + (z_r - \bar{z}_r)^2} \quad (14)$$

$$\eta_{rh}(t) = \sqrt{(x_r - x_h - \bar{x}_r + \bar{x}_h)^2 + (z_r - z_h - \bar{z}_r + \bar{z}_h)^2} \quad (15)$$

Parameters	Unit	Value
Mean wind speed	m/s	12
Turbulence intensity factor	—	0.146 (IEC Class C)
Water depth	m	30
Monopile foundation length	m	36
Monopile substructure length	m	30
Tower length	m	77.6
Position of the crane tip	m	$[0, 0, -110]^\top$
Yoke mass m_y	ton	20
Blade mass m_b	ton	17.74
Blade moment of inertia at COG I_b	kg · m^2	4.31e6
Blade length	m	62.5
Arms of the tugger line forces $[r_{t1}, r_{t2}, r_{t3}]$	m	$[-4.5, 4.5, -6.22]$
Length of lift wire	m	9.2
Stiffness of lift wire	N/m	5.59e8
Length of slings	m	9
Stiffness of slings	N/m	1e8
Lift wire and spring damping ratio	—	1%
Gain matrix of P controller K_p	—	diag{1e5, 1e7}
Gain matrix of D controller K_d	—	diag{1e4, 0.5e6}
Gain matrix of I controller K_i	—	diag{1e3, 3e5}
Weighting matrix Q_1	—	diag{100, 1}
Weighting matrix Q_2	—	diag{1e-7, 1e-7, 1e-7}

Table 1 Parameters used for numerical simulations

where x_r, z_r, x_h, and z_h define the positions of the blade root center and hub center, respectively.

CVXGEN is used for control allocation to calculate the control input on each tugger line f_c based on the desired system input τ_c. C++ codes are generated with an online interface, which ensures high computational speed. The calculation speed satisfies a real-time online optimization scenario.

Time-Domain Simulation Results

The time-domain simulation results are presented in Figs. 10–14. The position history of the blade root center is presented in Fig. 10, which shows that the blade's motion is greatly reduced by the proposed PID controller. The blade's motion in the inflow direction is also greatly reduced. The deviation of the blade root center position between the two schemes is caused by the wind loads. The starting positions for both schemes are the same, which corresponds to the positions without wind loads. In the passive scheme, the equilibrium position of the suspended blade has an offset from the starting position under the wind loads. For the active scheme, the active controller manages to stabilize the payload at its starting position. The position deviation is influenced by the mean wind speed. To cancel the derivation in the equilibrium positions, the only thing to do is to change the position of

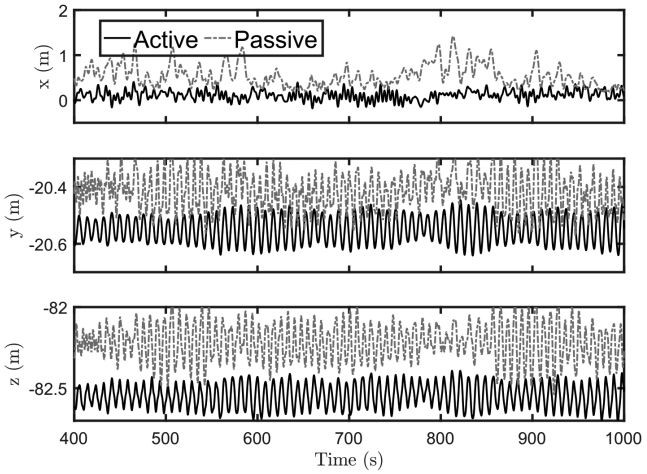

Fig. 10 Position of the blade root center, $U_w = 12$ m/s, $TI = 0.146$, $H_s = 2$ m, and $T_p = 6$ s

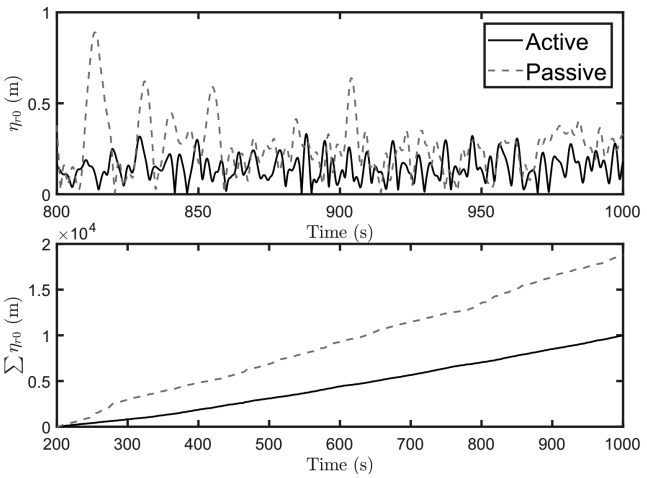

Fig. 11 Absolute motion radius history of the blade root center η_{r0} and accumulated error of the motion, $U_w = 12$ m/s, $TI = 0.146$, $H_s = 2$ m, and $T_p = 6$ s

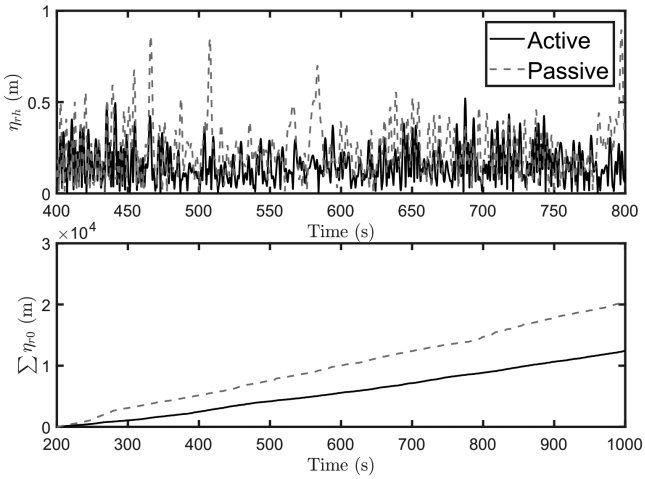

Fig. 12 Relative motion radius history between the hub and blade root center and accumulated error of the motion η_{rh}, $U_w = 12$ m/s, $TI = 0.146$, $H_s = 2$ m, and $T_p = 6$ s

the crane tip. The influence on the mating operation is considered negligible.

Figures 11 and 12 show that the motion radii of the active-control scheme are limited to a smaller range than the typical passive method. With a 100 Hz sampling frequency, the accumulated errors for the active scheme are much fewer than those for the passive configuration. Therefore, the proposed controller can reduce the blade's motion relative to the hub. High-frequency oscillations are found in Fig. 12 as a result of the wave-induced hub motions. It can be concluded that the proposed method effectively improves the installation success rate of the mating operations.

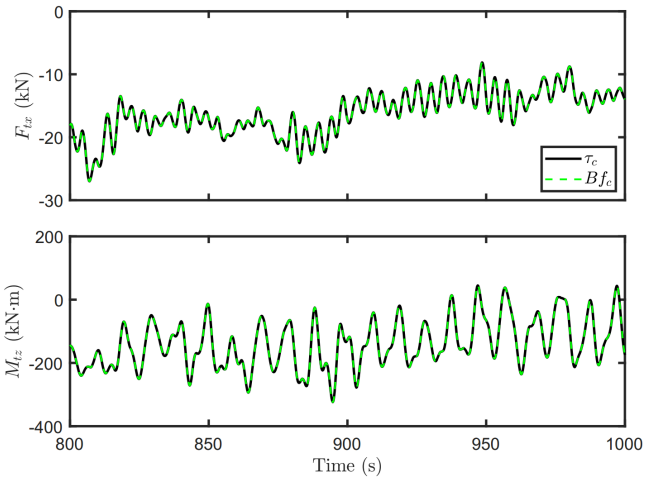

Fig. 13 Performance to track the desired control input τ_c and Bf_c, $U_w = 12$ m/s, $TI = 0.146$, $H_s = 2$ m, and $T_p = 6$ s

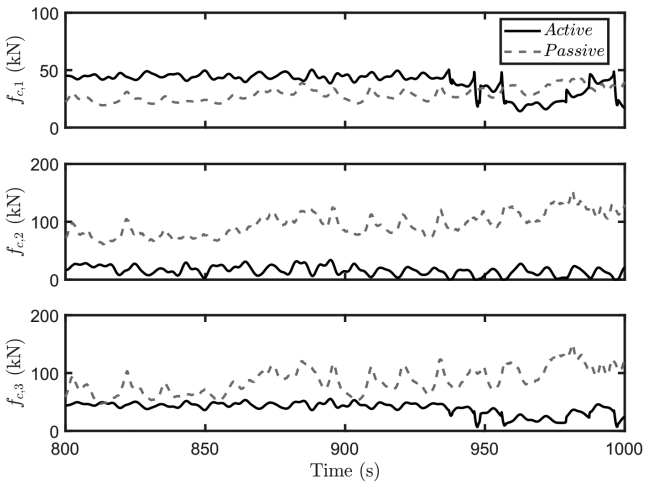

Fig. 14 History of the tension on the tugger lines f_c, $U_w = 12$ m/s, $TI = 0.146$, $H_s = 2$ m, and $T_p = 6$ s

Figure 13 presents the time-domain performance of the proposed control allocation approach. The achieved total load from command signals Bf_c follows the desired values τ_c well. Furthermore, the tension on each wire rope stays within a reasonable range with a limited rate of change; see Fig. 14. The tension on each tugger line is positive and under its limit. No sudden rise or drop is found. For the tugger lines 2 and 3, the tension in the active scheme is much smaller than that in the passive-installation approach. The tension on tugger line 1 is greater with the active controller. Thus, the control allocation module works well to provide the desired force and torque to the suspended blade.

CONCLUSIONS AND FUTURE RESEARCH

This paper proposes a closed-loop scheme for tugger line force control for single-blade installation. A PID controller is adopted to insert restoring, damping, and integral forces to the blade dynamics in the mean wind direction and the moment about the vertical axis. The placement of tugger lines is discussed, and it is shown that a third well-located tugger line increases the control space significantly. The control allocation is achieved with a convex programming solver.

To verify the performance of the controller, time-domain simulations are conducted in turbulent wind conditions using MATLAB and HAWC2. Motion radii are employed as the criteria to evaluate the controller's performance. The proposed active control scheme can stabilize the blade in turbulent wind. The performance of the active scheme is superior to that of the passive scheme.

In future work, other scenarios of single-blade installation will be addressed. For example, the flexibility of the crane tip should be considered the boundary condition of the lift wire. Furthermore, the span-wise motion should be canceled by the controller.

ACKNOWLEDGEMENTS

This work was supported by the Research Council of Norway (RCN) through the Centre for Research-Based Innovation on Marine Operations (CRI MOVE, RCN-project 237929).

REFERENCES

Åström, KJ, and Hägglund, T (1995). *PID Controllers: Theory, Design, and Tuning*, 2nd Ed, Instrumentation, Systems, and Automation Society, Research Triangle, NC, USA, 343 pp.

Bhattacharya, S, and Adhikari, S (2011). "Experimental Validation of Soil–Structure Interaction of Offshore Wind Turbines," *Soil Dyn Earthquake Eng*, 31(5-6), 805–816. https://doi.org/10.1016/j.soildyn.2011.01.004.

Cheng, X, et al. (2019a). "A Neural-Network-Based Sensitivity Analysis Approach for Data-Driven Modeling of Ship Motion," *IEEE J Oceanic Eng*, 1–11. https://doi.org/10.1109/JOE.2018.2882276.

Cheng, X, et al. (2019b). "Data-Driven Uncertainty and Sensitivity Analysis for Ship Motion Modeling in Offshore Operations," *Ocean Eng*, 179, 261–272. https://doi.org/10.1016/j.oceaneng.2019.03.014.

Deng, W, Liu, H, Xu, J, Zhao, H, and Song, Y (2020). "An Improved Quantum-Inspired Differential Evolution Algorithm for Deep Belief Network," *IEEE Trans Instrum Meas*. https://doi.org/10.1109/TIM.2020.2983233.

Deng, W, Xu, J, and Zhao, H (2019). "An Improved Ant Colony Optimization Algorithm Based on Hybrid Strategies for Scheduling Problem," *IEEE Access*, 7, 20281–20292. https://doi.org/10.1109/ACCESS.2019.2897580.

DNV (2000). *Environmental Conditions and Environmental Loads*, Recommended Practice C205, Det Norske Veritas, Høvik, Norway, 124 pp.

Egeland, O, and Gravdahl, JT (2002). *Modeling and Simulation for Automatic Control*, Marine Cybernetics, Trondheim, Norway, 657 pp.

Gaunaa, M, Bergami, L, Guntur, S, and Zahle, F (2014). "First-Order Aerodynamic and Aeroelastic Behavior of a Single-Blade Installation Setup," *J Phys Conf Series*, 524, 012073. https://doi.org/10.1088/1742-6596/524/1/012073.

Gaunaa, M, Heinz, J, and Skrzypiński, W (2016). "Toward an Engineering Model for the Aerodynamic Forces Acting on Wind Turbine Blades in Quasisteady Standstill and Blade Installation Situations," *J Phys Conf Series*, 753, 022007. https://doi.org/10.1088/1742-6596/753/2/022007.

IEC (2005). *Wind Turbine Generator Systems, Part 1: Safety Requirements*, International Standard IEC 61400-1, International Electrotechnical Commision, 1400–1401.

Jiang, Z, Gao, Z, Ren, Z, Li, Y, and Duan, L (2018). "A Parametric Study on the Final Blade Installation Process for Monopile Wind Turbines Under Rough Environmental Conditions," *Eng Struct*, 172, 1042–1056. https://doi.org/10.1016/j.engstruct.2018.04.078.

Jiang, Z, Hu, W, Dong, W, Gao, Z, and Ren, Z (2017). "Structural Reliability Analysis of Wind Turbines: A Review," *Energies*, 10(12), 2099. https://doi.org/10.3390/en10122099.

Johansen, TA, and Fossen, TI (2013). "Control Allocation: A Survey," *Automatica*, 49(5), 1087–1103. https://doi.org/10.1016/j.automatica.2013.01.035.

Jonkman, J, Butterfield, S, Musial, W, and Scott, G (2009). *Definition of a 5-MW Reference Wind Turbine for Offshore System Development*, Technical Report NREL/TP-500-38060, National Renewable Energy Laboratory, Golden, CO, USA.

Jonkman, J, Butterfield, S, Passon, P, et al. (2008). *Offshore Code Comparison Collaboration Within IEA Wind Annex XXIII: Phase II Results Regarding Monopile Foundation Modeling*, Conference Paper NREL/CP-500-42471. https://www.nrel.gov/docs/fy08osti/42471.pdf.

Kuijken, L (2015). *Single Blade Installation for Large Wind Turbines in Extreme Wind Conditions*, Master of Science Thesis, Technical University of Denmark/TU Delft.

Mann, J (1998). "Wind Field Simulation," *Probab Eng Mech*, 13(4), 269–282. https://doi.org/10.1016/S0266-8920(97)00036-2.

Mattingley, J (2011). *Code Generation for Embedded Convex Optimization*, Thesis Dissertation, Stanford University, Palo Alto, CA, USA. https://purl.stanford.edu/qd834ss0073.

Moné, C, et al. (2017). *2015 Cost of Wind Energy Review*, Technical Report NREL/TP-6A2066861, National Renewable Energy Laboratory, Golden, CO, USA.

Ren, Z, Jiang, Z, Gao, Z, and Skjetne, R (2018a). "Active Tugger Line Force Control for Single Blade Installation," *Wind Energy*, 21(12), 1344–1358. https://doi.org/10.1002/we.2258.

Ren, Z, Jiang, Z, Skjetne, R, and Gao, Z (2018b). "Development and Application of a Simulator for Offshore Wind Turbine Blades Installation," *Ocean Eng*, 166, 380–395. https://doi.org/10.1016/j.oceaneng.2018.05.011.

Ren, Z, Skjetne, R, and Gao, Z (2019). "A Crane Overload Protection Controller for Blade Lifting Operation Based on Model Predictive Control," *Energie*s, 12(1), 50. https://doi.org/10.3390/en12010050.

Ren, Z, Skjetne, R, Jiang, Z, Gao, Z, and Verma, AS (2019). "Integrated GNSS/IMU Hub Motion Estimator for Offshore Wind Turbine Blade Installation," *Mech Syst Signal Process*, 123, 222–243. https://doi.org/10.1016/j.ymssp.2019.01.008.

RWE Innogy GmbH (2014). *Halfway Through the Turbine Installation for the Nordsee Ost Offshore Wind Farm*, Retrieved from https://w3.windfair.net/wind-energy/news/16711-halfway-through-the-turbine-installation-for-the-nordsee-ost-offshore-wind-farm.

Verma, AS, Jiang, Z, Ren, Z, Gao, Z, and Vedvik, NP (2019a). "Response-Based Assessment of Operational Limits for Mating Blades on Monopile-Type Offshore Wind Turbines," *Energies*, 12(10), 1867. https://doi.org/10.3390/en12101867.

Verma, AS, Jiang, Z, Vedvik, NP, Gao, Z, and Ren, Z (2019b). "Impact Assessment of a Wind Turbine Blade Root During an Offshore Mating Process," *Eng Struct*, 180, 205–222. https://doi.org/10.1016/j.engstruct.2018.11.012.

Zhen, X, Vinnem, JE, Yang, X, and Huang, Y (2019). "Quantitative Risk Modelling in the Offshore Petroleum Industry: Integration of Human and Organizational Factors," *Ships Offshore Struct*, 15(1), 1–18. https://doi.org/10.1080/17445302.2019.1589772.

Zhou, L, Gao, J, and Li, D (2019). "An Engineering Method for Simulating Dynamic Interaction of Moored Ship with First-Year Ice Ridge," *Ocean Eng*, 171, 417–428. https://doi.org/10.1016/j.oceaneng.2018.11.027.